Analysis of THz generation through the asymmetry of photoelectron angular distributions

Zhaoyan Zhou,[1,2,*] Xu Wang,[3] and C. D. Lin[1]

[1]*Department of Physics, Cardwell Hall, Kansas State University, Manhattan, Kansas 66506, USA*

[2]*Department of Physics, College of Science, National University of Defense Technology, 410073 Changsha, People's Republic of China*

[3]*Graduate School, China Academy of Engineering Physics, Beijing 100193, People's Republic of China*

(Received 24 January 2017; published 17 March 2017)

We analyze the mechanism of THz generation in a gas medium with intense two-color infrared lasers pulses. The dependence of the amplitude of THz emission on the relative phase between the fundamental color (800 nm) and its second harmonic (400 nm) is shown to be identical to the residual current as well as to the asymmetry of the above-threshold-ionization (ATI) photoelectrons along the left versus the right side of the linear polarization axis of the laser, thus confirming the validity of the semiclassical photocurrent model for the THz emission. We further analyze the even vs odd angular momentum distributions of the ATI electrons. The degree of overlap between the even-parity dominant electrons and the odd-parity dominant electrons within each ATI peak determines the strength of the THz emission, thus favoring the model that THz is generated through free-free transitions in the laser field. A model is also provided to obtain the same phase dependence as the four-wave mixing model.

DOI: 10.1103/PhysRevA.95.033418

I. INTRODUCTION

Terahertz (THz) radiation, due to its low photon energies, in general does not damage DNA and tissues. It can penetrate fabrics and plastics and has been used in medical imaging and security [1,2]. In recent years, time-domain THz spectroscopy has been used to study chemistry, biochemistry, and condensed medium and has been used in information and communications. With increasing power and shorter durations down to single or half-cycle, THz sources are now capable of driving nonlinear phenomena [3,4]. In the past decade, it has been found that efficient THz can be generated using gas-phase atoms and molecules [5,6]. In the low-pressure limit, THz is generated from individual gas target atoms or molecules. However, unlike the better-known high-order harmonic generation, the mechanism of THz emission is still under debate. Two popular mechanisms are generally accepted: one is the photocurrent (PC) model [7,8], and the other is a third-order nonlinear four-wave mixing (FWM) model [5,9]. The PC model relies on residual currents in the laser-atom interaction, while the FWM relies on the polarization of the medium.

It is well-known that THz generation by a single-color laser is very small, but it is very efficiently generated by using a two-color pulse [10–14]. So far, the evidence supports the photocurrent model, in that ionization of the medium is indispensable [13,14], yet the mechanism behind the generation of THz remains unclear. A lot of theoretical calculations have been carried out in the past ten years by solving the time-dependent Schrödinger equation (TDSE) [8,15–18] to study the THz signals versus the phase between the two colors of the laser, the intensity of the fundamental and of the second harmonic [17–19]. These TDSE calculations have shown consistent results among the studies, but the underlying mechanism remains unclear. While it has been speculated that THz emission can be attributed to the continuum-continuum transition during laser-assisted soft collision of the ionized electron with the atomic core [16,19,20], there is no clear demonstration how this model works.

In this paper, we analyze the intermediate results from the TDSE calculation to test the photocurrent model and interpret how THz emission can be attributed to continuum-continuum transitions. We carried out the analysis by linking the residual photocurrent to the asymmetry of the above-threshold ionization (ATI) photoelectrons in a two-color field. We show that the asymmetry of the photoelectron along the positive side vs the negative side of the laser polarization depends on the phase angle φ between the two colors of the laser. The same dependence was observed on the THz yield. We further analyze the even vs odd angular momentum distributions of the ATI electrons versus φ. For φ that leads to a large THz yield; the weights of even versus odd angular momenta at each ATI peak are very similar. We attribute THz emission to the laser-induced transitions between even and odd continuum states within the same ATI peak, thus leading to low-energy THz photons. The observed near-cos φ dependence of the THz emission is modeled, which has the same cos φ dependence but it has nothing to do with the four-wave mixing model.

In the remainder of the paper, next we explain how the calculations were carried out. Then the main results are presented together with discussion on the theoretical model. The last section concludes the finding of this work.

II. THEORETICAL METHODS

We calculate the THz spectrum and the photoelectron momentum spectra by carrying out the numerical solution of the TDSE (in atomic units),

$$i\frac{\partial}{\partial t}\psi(\mathbf{r},t) = (\hat{H}_0 + \hat{H}_I)\psi(\mathbf{r},t), \tag{1}$$

where $\hat{H}_0$ is the field-free Hamiltonian and $\hat{H}_I$ is the interaction part given in the length gauge. In the dipole approximation,

$$\hat{H}_I = -\mathbf{E}_\mathbf{L}\cdot\mathbf{r}\,f(t)[\cos(\omega t) + 0.1\cos(2\omega t + \varphi)], \tag{2}$$

where the envelope of the laser pulse, $f(t)$, is chosen to be of sine-square form with 20 optical cycles (o.c.) in duration.

*zhaoyanz@phys.ksu.edu

E_L is the amplitude of the 800-nm fundamental laser field and the second-order harmonic field (400 nm) has 10% amplitude of the fundamental one. The 400-nm laser pulse alone is too weak to ionize the atom. Linearly polarized laser pulses are considered throughout the investigation; thus we only need to consider the $m = 0$ component of the magnetic quantum number of the atom. We study the THz generation and the left ($z < 0$) and right ($z > 0$) asymmetry in the photoelectron energy spectra vs the relative phase delay φ of the two-color fields.

The time-dependent wave function is expanded with Legendre polynomials in the θ coordinate as

$$\psi(r_i,x_j,t) = \sum_{l=0}^{L} c_l(t)R_l(r_i)P_l(x_j), x_j = \cos\theta_j, \quad (3)$$

and the radial function $R_l(r)$ is expanded using the discrete variable representation (DVR) basis set associated with Legendre polynomials [21–23]. The coefficients c_l can be calculated using the split-operator method [24]. Here we expand the wave functions with 4000 DVR points for $r_{\max} = 2000$ a.u. and 120 partial waves. Once the time-dependent wave function is determined, the induced dipole moment is calculated using the acceleration form

$$a(t) = \langle\psi(\mathbf{r},t)|\frac{\partial V}{\partial z}|\psi(\mathbf{r},t)\rangle. \quad (4)$$

The emission spectrum including the THz emission can be obtained by the Fourier transformation of the time-dependent dipole moment [16]. To obtain the THz spectrum without continuing the calculation to the long time of about 5 ps, we use the wavelet analysis to sample the frequency of the radiation in the THz region. This is performed by a wavelet transformation [25],

$$A_\omega(t_0,\omega) = \int a(t)w_{t_0,\omega}(t)dt, \quad (5)$$

with the wavelet kernel $w_{t_0,\omega}(t) = \sqrt{\omega}W[\omega(t - t_0)]$, where $W[x] = \frac{1}{\sqrt{\tau}}e^{ix}e^{-x^2/2\tau^2}$. τ is chosen to be 5 a.u. and ω is 18 THz (0.0028 a.u.), which is the peak frequency of the THz wave studied here [26]. The THz wave emits throughout the whole laser pulse [16] as shown in Fig. 1. We take its peak as the THz emission amplitude.

According to the classical photocurrent model, the residual current is responsible for the generation of the THz wave. One can estimate the emission amplitude by the value of the total current. From the time-dependent wave function, the electron current density in the direction of polarization is given by $j(t) \propto \int_0^t a(t)dt$, from which the residual current is obtained:

$$J_{\mathrm{RCD}} = \frac{1}{T}\int_0^T j(t)dt. \quad (6)$$

The two-color field in Eq. (2) also will result in asymmetric photoelectron spectrum. The two-dimensional (2D) electron momentum distribution can be calculated by projecting out the final time-dependent wave function at the end of the laser pulse to the eigenstates of the continuum electron of momentum $\mathbf{p}$ [27]:

$$\frac{\partial^2 P}{\partial E\partial\theta} = |\langle\Phi_p^-|\psi(t = t_f)\rangle|^2 2\pi p\sin\theta, \quad (7)$$

where $E = p^2/2$ is the kinetic energy of the photoelectron and θ is the angle between the momentum vector $\mathbf{p}$ and the laser polarization directions (along the z axis). The electron energy spectrum can be obtained by integrating over θ:

$$\frac{\partial P}{\partial E} = \int \frac{\partial^2 P}{\partial E\partial\theta}d\theta. \quad (8)$$

We can also calculate the ATI spectrum in $\pm z$ sides from Eq. (8) by setting the integration range to be $0 \sim \pi/2$ and $\pi/2 \sim \pi$, respectively. The asymmetry of the photoelectron [28,29] is then defined by the A coefficient:

$$A = (P_+ - P_-)/(P_+ + P_-). \quad (9)$$

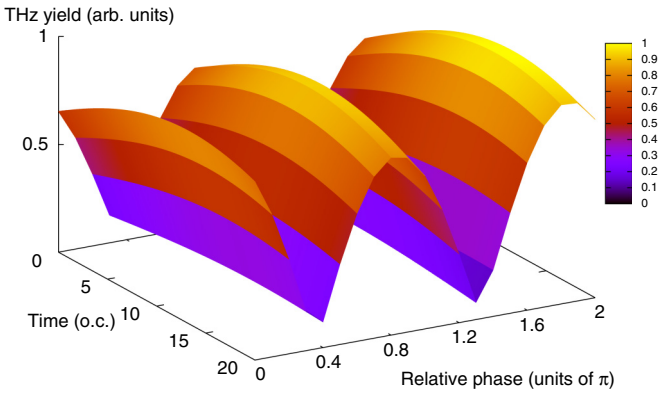

FIG. 1. The time profile of the 18 THz for H atoms in 20-o.c. two-color laser fields for different relative phases φ. The intensity of the fundamental laser field is 1.0×10^{14} W/cm^2 and the second-order one is 1% intensity of the fundamental one.

III. RESULTS AND DISCUSSION

As stated in the Introduction, our goal is to analyze the TDSE results to provide a glimpse of the validity and limitation of the simple photocurrent model as well as the simple four-wave mixing model. We first make a calculation for hydrogen atoms with the intensity of the fundamental laser field set at 1.0×10^{14} W/cm^2. The dependence of the THz amplitude on the relative phase φ is shown in Fig. 2(a). The φ dependence of the THz amplitude, of the asymmetry of the total photoelectrons, and of the total residual photocurrent calculated quantum mechanically all lie on top of each other. Note that both the THz amplitude and the asymmetry of photoelectron are measurable quantities. This establishes the close relation between the THz generation and the asymmetry of photoelectrons on the two sides ($+z$ and $-z$) of the polarization axis. It also establishes the validity of the residual photocurrent model, except that the current has to be calculated quantum mechanically, not by the simple classical model. For the present example, maximal THz occurs when the phase $\varphi = 0.9\ \pi$. Minimum THz generation occurs at $\varphi = 0.4\ \pi$. Figure 2(b) shows the ATI spectrum on the right side ($+z$) and on the left side ($-z$) overlap very well, such that the residual

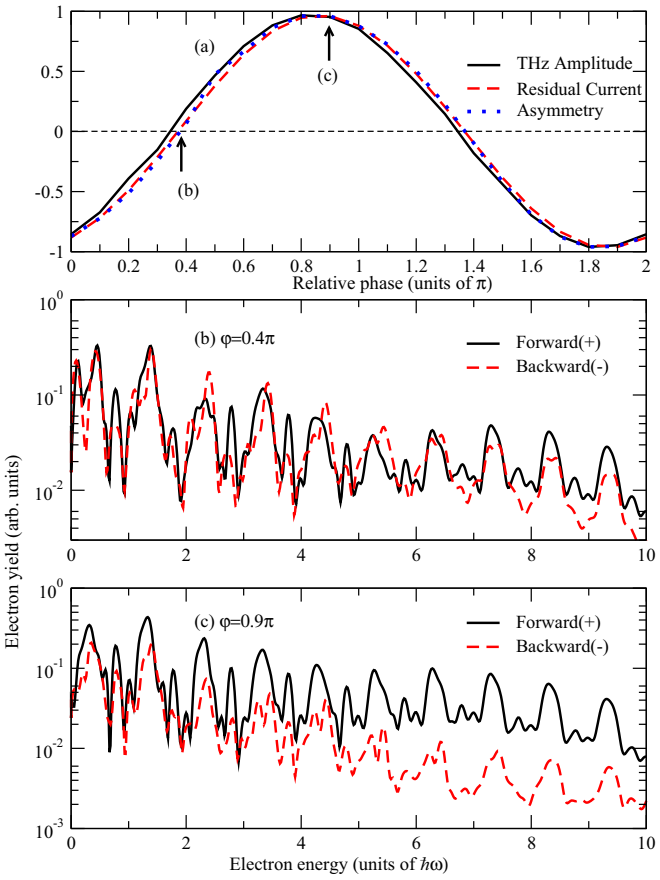

FIG. 2. (a) The normalized THz emissions (solid black line), the residual photocurrent (dashed red line), and the asymmetry parameter (dotted blue line) as a function of the relative phase of the fundamental (800 nm) laser field and its second harmonic (400 nm) laser field. The laser parameters are the same as those in Fig. 1. The yields of the ATI electron on the right side ($z > 0$, solid black line) and on the left side ($z < 0$, dashed red line) are shown in panel (b) for $\varphi = 0.4\,\pi$ and in (c) for $\varphi = 0.9\,\pi$, where the THz yield in panel (a) is at the minimum and the maximum, respectively.

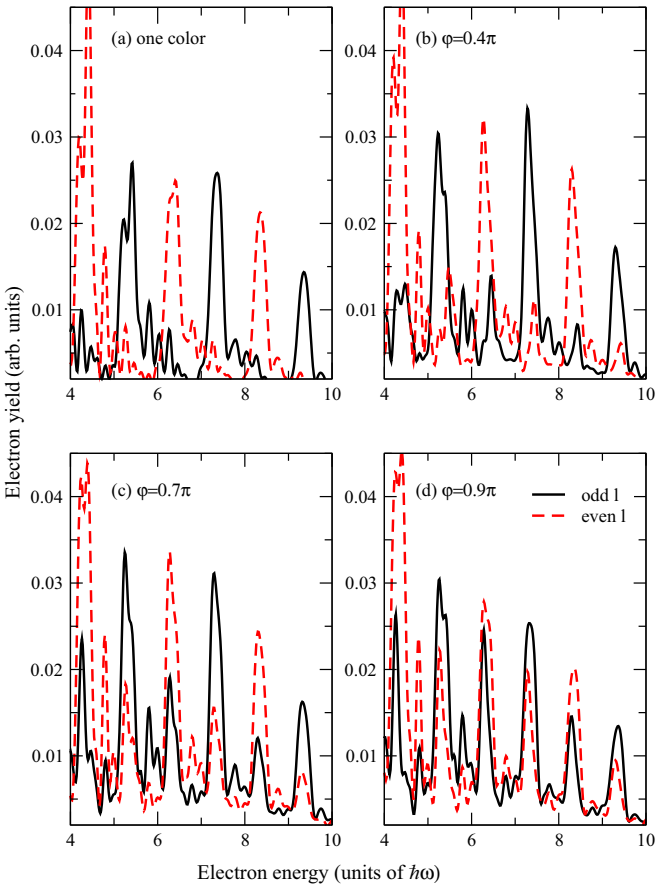

FIG. 3. The ATI spectra of electron with even (solid black line) and odd (dashed red line) integer orbital quantum numbers along the polarization direction for (a) a monochromatic 800-nm laser field and two-color laser fields when (b) $\varphi = 0.4\,\pi$, (c) $\varphi = 0.7\,\pi$, and (d) $\varphi = 0.9\,\pi$. The odd-even mixture degree increases from panel (a) to panel (d) when the THz yield gets stronger. Laser parameters are the same as those in Fig. 1.

current is at the minimum. On the other hand, in Fig. 2(c), the ATI peaks on the right side are much stronger than those on the left side, especially for higher ATI peaks, thus resulting in a high residual current.

Figure 2(a) shows that the maximum THz amplitude occurs at $\varphi = 0.9\,\pi$ and the zero amplitude occurs near $\varphi = 0.4\,\pi$. The relative phase φ dependence is closer to the prediction of the four-wave mixing model [25,26]. In this model, the third-order optical nonlinear effect is used to describe the parametric conversion from laser fields to THz emissions and the THz emissions can be approximated by

$$E_{\mathrm{THz}} \propto \chi^{(3)} \sqrt{I_{2\omega}} I_{\omega} \cos\varphi, \tag{10}$$

where I_{ω} and $I_{2\omega}$ are the intensity of the incident fundamental and its second harmonic, and $\chi^{(3)}$ is the third-order nonlinearity. However, at the intensity used for the gas target considered here, the multiphoton or tunneling model is more appropriate for describing the ionization and the generation of high-order harmonics; the pure four-wave mixing model is not applicable. In view of the good agreement between the residual current model and the THz amplitude in Fig. 2(a), it is also desirable to provide a connection between the electron energy distribution and the THz emission.

How does a partially ionized medium give rise to the THz emission? For this purpose, we analyze the even and odd character of the wave function of the ATI photoelectron. This can be done by expressing the composition for each ATI electron into even-integer orbital quantum numbers and odd-integer orbital quantum numbers. Figure 3(a) shows the even or odd compositions for a single-color laser. Each ATI peak is dominated by an even composition or an odd composition. The lack of even-odd mixing thus guarantees that the photoelectron spectra do not exhibit forward and backward asymmetry, as one can expect for ionization from a 20-o.c. laser pulse. We next analyze the even-odd composition of the ATI peaks for the two-color fields given in Eq. (2). For $\varphi = 0.4\,\pi$, as shown in Fig. 3(b), the even-odd mixing is quite small, thus it is quite similar to the single-color case shown in Fig. 3(a). This is the case where the THz generation is very weak. In Fig. 3(c), where $\varphi = 0.7\,\pi$, we observe that the even-odd mixture becomes more prominent, with the weaker component less than 50% of the main one. For $\varphi = 0.9\,\pi$, the even-odd mixture is nearly

equal. This is when the THz generation is at its maximum. This observation leads us to attribute THz generation to the degree of even-odd angular momentum mixing of the continuum wave function of the photoelectrons. Since each ATI peak has a narrow bandwidth, there is a dipole-allowed transition between the even part of a continuum electron with energy $E+\epsilon$ and the odd part of a continuum electron with energy E, with the emission of a THz photon with energy ϵ. This is an extension of the photocurrent model using the quantum picture where THz generation is attributed to the emission of radiation between nearly degenerate continuum electrons (Although these are the energy distributions of electrons at the end of the laser pulse, we did not find an obvious difference when the ATI spectra were plotted at 18 or 19 o.c. of the laser pulse).

To reach high THz yield, the even and odd components of the orbital angular momentum distributions should be as close to each other as possible to achieve maximal asymmetry of the photoelectron distributions. The electrons from the fifth and the tenth ATI peaks contribute most to its asymmetry as shown in Fig. 2(c) and the odd-even mixture is more evident for these ATI peaks. This analysis further allows us to identify which part of the ionized electrons contributes most to the THz emission.

Based on the nature of ATI electron's wave function, can we explain qualitatively the near-$\cos\varphi$ dependence of the THz amplitude? In a multiphoton ionization picture, a final state u_{f_1} can be reached from some intermediate state u_i by absorbing one 2ω photon or from the same intermediate state by absorbing two ω photons to reach a nearby state u_{f_2}. The amplitude for reaching each final state is given by

$$a^{(1)}_{f_1 i} = -i\int_{t_0}^{t}\langle u_{f_1}|H_i(t_1)|u_i\rangle e^{i(E_{f_1}-E_i)t_1}dt_1 \tag{11}$$

and

$$a^{(2)}_{f_2 i} = (-i)^2\int_{t_0}^{t}dt_1\int_{t_0}^{t_1}dt_2 e^{-iE_{f_2}t_1}\langle u_{f_2}|H_i(t_1)|u_{k_1}\rangle \times e^{-iE_{k_1}(t_2-t_1)}\langle u_{k_1}|H_i(t_2)|u_i\rangle e^{-iE_i t_2}, \tag{12}$$

respectively. Setting the initial and final time to infinity, we obtain

$$a^{(1)}_{f_1 i} = -2\pi i\frac{E_{2\omega}}{2}e^{-i\varphi}M_{f_1 i}\delta(E_{f_1}-E_i-2\omega),$$
$$M_{f_1 i} = \langle u_{f_1}|z|u_i\rangle, \tag{13}$$

and

$$a^{(2)}_{f_2 i} = 2\pi i\frac{E^2_\omega}{4}T^{(2)}_{f_2 i}\delta(E_{f_2}-E_i-2\omega),$$
$$T^{(2)}_{f_2 i} = \sum_{k_1}\frac{\langle u_{f_2}|z|u_k\rangle\langle u_k|z|u_i\rangle}{E_i+\omega-E_{f_2}}. \tag{14}$$

For THz emission, the transition dipole from u_{f_1} to u_{f_2} is

$$d_x(t) = \langle u_{f_2}|z|u_{f_1}\rangle + \langle u_{f_1}|z|u_{f_2}\rangle = 2\mathrm{Re}(\langle u_{f_1}|z|u_{f_2}\rangle) \propto \mathrm{Re}\big(a^{(1)*}_{f_1 i}a^{(2)}_{f_2 i}\big). \tag{15}$$

Inserting Eqs. (13) and (14), we can get

$$d_x(t) \propto E^2_\omega E_{2\omega}\cos\varphi. \tag{16}$$

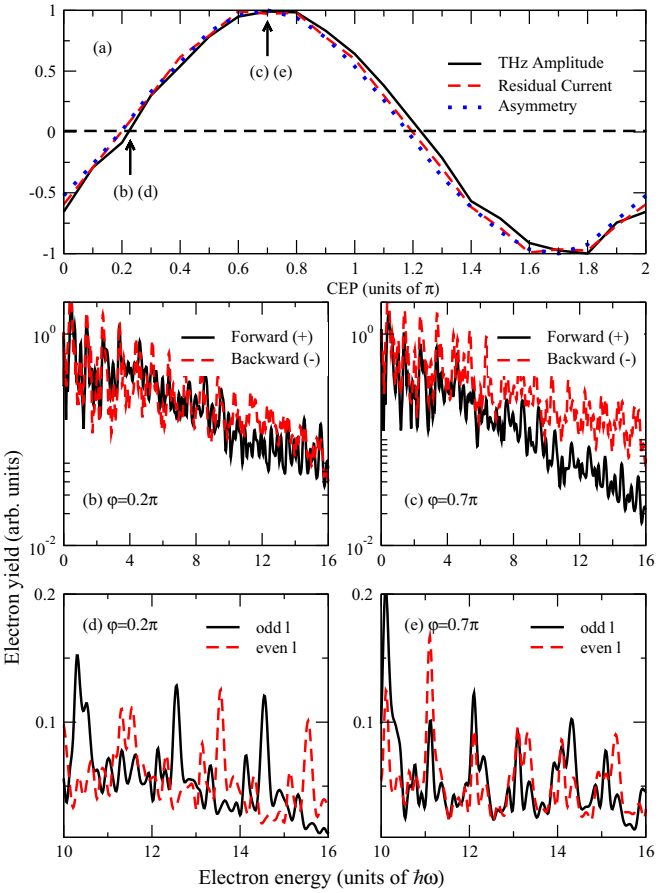

FIG. 4. (a) The normalized THz emissions (solid black line), the residual photocurrent (dashed red line), and the asymmetry parameter (dotted blue line) as a function of the relative phase of the fundamental laser (800 nm) and its second harmonic (400 nm). The intensity of the fundamental laser is 2.26×10^{14} W/cm^2 and the second harmonic intensity is 1% of the fundamental. The total ATI spectra on the right and left of the polarization axis are given in panel (b) for $\varphi=0.2\,\pi$ and in panel (c) for $\varphi=0.7\,\pi$ when the asymmetry of the total ATI spectrum reaches its minimum and maximum, respectively. The corresponding even (solid black line) and odd (dashed line) angular orbital momentum distributions for $\varphi=0.2\,\pi$ and $\varphi=0.7\,\pi$ are shown in panels (d) and (e), respectively.

This has the same expression as the four-wave mixing model. In this model, we emphasize that THz generation comes from dipole transition between continuum states near each ATI peak. The simple expression in the last equation is correct only if the intermediate state is not affected by the driving laser. This of course is not correct. The effect of the two-color laser on the intermediate state will introduce modification to the expression in Eq. (16). Thus the peak of the THz is not maximum at $\varphi=1.0\,\pi$, but rather at $\varphi=0.9\,\pi$ for example, and will be intensity dependent [17,18].

Similar analysis can be applied to THz and 2D electron momentum spectra generated for atomic hydrogen by a two-color pulse where the intensity of the fundamental is raised to 2.26×10^{14} W/cm^2. Figure 4(a) compares the THz amplitude, the residual current, and the asymmetry of the ATI electrons. The three curves agree with each other quite

well. The peak amplitude is at $\varphi = 0.7\,\pi$, and the near-zero amplitude occurs at $\varphi = 0.2\,\pi$, moving closer toward the $\sin\varphi$ dependence predicted by the classical photocurrent model. On the other hand, the electron distribution and the even-odd angular momentum distributions behave similarly to those in Fig. 2 at the lower laser intensity. This establishes that the underlying reason of understanding the φ dependence of THz and of the asymmetry of photoelectron is correct. The photocurrent model is basically sound but the current has to be calculated quantum mechanically.

IV. CONCLUSIONS

In this article, we analyzed the THz generation of atomic hydrogen by a 20-o.c. two-color laser pulse, consisting of an 800-nm laser with a 400-nm laser with 1% of the intensity of the fundamental. The phase φ values between the two colors are varied over the 2π range. We used the TDSE to calculate the THz generation and to obtain the photoelectron momentum spectrum. We have found that THz and the asymmetry of the photoelectron distributions have identical dependence, thus allowing us to draw a firm conclusion that the mechanism of THz generation follows the photocurrent model. By analyzing the angular momentum distributions of the ATI electrons, we further propose that THz generation is due to the laser-driven free-free transitions within each ATI peak. The near-$\cos\varphi$ dependence of THz emission is further understood in terms of the multiphoton ionization model. In this model, the near-$\cos\varphi$ dependence is attributed to continuum-continuum transition where the even-ℓ vs odd-ℓ continuum states are populated by a 400-nm photon or two 800-nm photons. The transition between these even-ℓ and odd-ℓ states results in the THz spectra and its $\cos\varphi$ dependence. This dependence has nothing to do with the derivation based on the four-wave mixing model. In the future, THz measurement should be carried out in coincidence with the asymmetry of the photoelectron momentum distribution to shed light directly on the interpretation presented in this paper.

We point out that circular polarized two-color laser fields have been used recently to generate THz waves [11,30]. It was found that, if the circular polarizations of the two colors are the same, the THz generation is about four times more efficient than if both colors have linear polarizations. Since rescattering is absent for circularly polarized lights, we can safely conclude that rescattering plays no role in THz generation, in contrast to high-harmonic generation where rescattering is dominant. It would be interesting to investigate how to extend the present analysis to THz generation by circular-polarized two-color fields where the magnetic quantum number m of a photoelectron is not fixed.

ACKNOWLEDGMENTS

Z.Y.Z. would like to thank the hosting of the J. R. MacDonald Laboratory at Kansas State University where this work was carried out. C.D.L. is supported in part by Chemical Sciences, Geosciences and Biosciences Division, Office of Basic Energy Sciences, Office of Science, U.S. Department of Energy, under Grant No. DE-FG02-86ER13491.

[1] M. Tonouchi, Nat. Photonics **1**, 97 (2007).
[2] J. F. Federici, B. Schulkin, F. Huang, D. Gary, R. Barat, F. Oliveira, and D. Zimdars, Semicond. Sci. Technol. **20**, S266 (2005).
[3] K. Kovács, E. Balogh, J. Hebling, V. Tosa, and K. Varjú, Phys. Rev. Lett. **108**, 193903 (2012).
[4] E. Balogh, K. Kovacs, P. Dombi, J. A. Fulop, G. Farkas, J. Hebling, V. Tosa, and K. Varju, Phys. Rev. A **84**, 023806 (2011).
[5] X. Xie, J. Dai, and X.-C. Zhang, Phys. Rev. Lett. **96**, 075005 (2006).
[6] J. Dai, X. Xie, and X.-C. Zhang, Phys. Rev. Lett. **97**, 103903 (2006).
[7] K. Kim, J. H. Glownia, A. J. Taylor, and G. Rodriguez, Opt. Express **15**, 4577 (2007).
[8] A. A. Silaev and N. V. Vvedenskii, Phys. Rev. Lett. **102**, 115005 (2009).
[9] D. J. Cook and R. M. Hochstrasser, Opt. Lett. **25**, 1210 (2000).
[10] M. D. Thomson, V. Blank, and H. G. Roskos, Opt. Express **18**, 023173 (2010).
[11] J. Dai, N. Karpowicz, and X.-C. Zhang, Phys. Rev. Lett. **103**, 023001 (2009).
[12] M. Kress, T. Löffer, S. Eden, M. Thomson, and H. G. Roskos, Opt. Lett. **29**, 1120 (2004).
[13] Y. S. You, T. I. Oh, and K. Y. Kim, Phys. Rev. Lett. **109**, 183902 (2012).
[14] T. Löffler, M. Kress, M. Thomson, and H. G. Roskos, Acta. Phys. Pol. A **107**, 99 (2005).
[15] N. Karpowicz and X.-C. Zhang, Phys. Rev. Lett. **102**, 093001 (2009).
[16] Z. Zhou, D. Zhang, Z. Zhao, and J. Yuan, Phys. Rev. A **79**, 063413 (2009).
[17] A. A. Silaev, M. Y. Ryabikin, and N. V. Vvedenskii, Phys. Rev. A **82**, 033416 (2010).
[18] W. Chen, Y. Huang, C. Meng, J. Liu, Z. Zhou, D. Zhang, J. Yuan, and Z. Zhao, Phys. Rev. A **92**, 033410 (2015).
[19] D. Zhang, Z. Lu, C. Meng, X. Du, Z. Zhou, Z. Zhao, and J. Yuan, Phys. Rev. Lett. **109**, 243002 (2012).
[20] Z. Lv, D. Zhang, C. Meng, X. Du, Z. Zhou, Y. Huang, Z. Zhao, and J. Yuan, J. Phys. B: At. Mol. Opt. Phys. **46**, 155602 (2013).
[21] D. O. Harris, G. G. Engerholm, and W. D. Gwinn, J. Chem. Phys. **43**, 1515 (1965).
[22] A. S. Dickinson and P. R. Certain, J. Chem. Phys. **49**, 4209 (1968).
[23] J. C. Light and R. B. Walker, J. Chem. Phys. **65**, 4272 (1976).
[24] X. M. Tong and S.-I Chu, Chem. Phys. **217**, 119 (1997).
[25] X. M. Tong and S.-I Chu, Phys. Rev. A **61**, 021802(R) (2000).
[26] T. Bartel, P. Gaal, K. Reimann, M. Woerner, and T. Elsaesser, Opt. Lett. **30**, 2805 (2005).

[27] Z. Chen, T. Morishita, A. T. Le, M. Wickenhauser, X. M. Tong, and C. D. Lin, Phys. Rev. A **74**, 053405 (2006).
[28] S. Chelkowski, A. D. Bandrauk, and A. Apolonski, Phys. Rev. A **70**, 013815 (2004).
[29] X. Zheng, M.-M. Liu, H. Xie, P. Ge, M. Li, and Y. Liu, Phys. Rev. A **92**, 053422 (2015).
[30] C. Meng, W. Chen, X. Wang, Z. Lv, Y. Huang, J. Liu, D. Zhang, Z. Zhao, and J. Yuan, Appl. Phys. Lett. **109**, 131105 (2016).